NASA Contractor Report 185190
AIAA-90-0740

Primary Arm Spacing in Directionally Solidified Pb–10 wt % Sn Alloys

M. A. Chopra and S. N. Tewari
Cleveland State University
Cleveland, Ohio

January 1990

Prepared for
Lewis Research Center
Under Cooperative Agreement NCC3–95

NASA

PRIMARY ARM SPACING IN DIRECTIONALLY SOLIDIFIED Pb-10 wt % Sn ALLOYS

M.A. Chopra* and S.N. Tewari†
Cleveland State University
Chemical Engineering Department
Cleveland, Ohio 44115

SUMMARY

The dependence of primary arm spacings on growth speed has been investigated for cellular and dendritic arrays in Pb-10 wt % Sn samples directionally solidified under a constant positive thermal gradient in the melt. The gradient of constitutional supercooling has been varied from almost zero (near the break-down of the planar liquid-solid interface at small growth speeds, cellular morphology) to near unity (large growth speeds, dendritic morphology). The spatial arrangements of cells and dendrites, as given by their co-ordination number, are not very different from each other. It appears that primary arm spacing maxima and the cell to dendrite transition are strongly influenced by the magnitude of the solute partition coefficient. The planar to cellular bifurcation in Pb-Sn, which is supercritical, has a high partition coefficient, as compared to the subcritical behavior reported in Al-Cu and succinonitrile-acetone which both have low partition coefficients. The primary arm spacing model due to Hunt agrees with the experimentally observed trend for the whole growth regime. There is a good quantitative agreement at higher gradients of supercooling. However, the model overpredicts the primary arm spacings at low gradients of constitutional supercooling.

INTRODUCTION

The microstructure at the liquid-solid interface during directional solidification in a positive thermal gradient is planar, cellular or dendritic depending upon the gradient of constitutional supercooling. The parameter, $(1 - S^*)$, where $S^* = [D_l G k/m_l R C_o(k - 1)]$, has been used (refs. 1 and 2) to indicate the gradient of constitutional supercooling for binary alloys. Here D_l is the solute diffusivity in the melt, G, the effective thermal gradient at the liquid-solid interface, k, the solute partition coefficient, m_l, the slope of the liquidus line from the phase diagram, R the growth speed and C_o is the solute content of the melt. For a given thermal gradient as the growth speed increases, the value of $(1 - S^*)$ increases from zero for a planar liquid-solid interface to its maximum value of one, as the microstructure first becomes cellular and then dendritic. The growth rate and thermal gradient dependence of primary arm spacings (λ_l) have been extensively investigated in the literature (refs. 3 to 20). Figure 1, a schematic representation of the growth rate dependence of primary arm spacings, summarizes the behaviors which have been experimentally observed. As the growth speed increases from R_p, the growth speed for the initial break-down of a planar liquid-solid interface, the primary arm spacings decrease in region A. A minimum in primary arm spacings occurs at a growth speed denoted as R_{min}. With further increase in growth

---

*NASA Resident Research Scientist at Lewis Research Center.
†Associate Professor.

speed, the spacings increase in region B, till a maximum is reached at R_{max}, beyond which they decrease in region C. Region C represents the most extensively investigated growth regime (refs. 3 to 11). Behavior shown near R_{max} has also been reported in several alloy systems (refs. 4 to 6 and 12 to 16). The primary arm spacing minimum, near R_{min}, has been reported in Al-4 wt % Cu (ref. 13) and succinonitrile-acetone (ref. 17). The decreasing arm spacing behavior near R_p has been observed in Pb-Tl (ref. 18) and succinonitrile-acetone (ref. 17). However, only for succinonitrile-acetone, has the complete growth regime from R_p to beyond R_{max} been investigated in a systematic manner. Otherwise, the individual experiments have concentrated either in region A near R_p (refs. 18 and 19) or in region C with some portion of B included (refs. 12 to 16). Only one metallic binary, Al-Cu, has been studied in all the three regions (refs. 8 to 10 and 13, 14, 19). However, contradictory behaviors are reported in Al-Cu investigations. Sharp and Hellawell (ref. 19) report that the primary arm spacings for the cellular microstructures are independent of the growth speed, and that these increase sharply when the structure becomes "branched-cell"; with a subsequent decrease at higher growth speeds. Miyata et al. (ref. 13) report an initial decrease in primary arm spacings with increasing growth speed near R_{min} for the cellular array, a slow increase to a maximum near R_{max} and the usually observed decreasing trend beyond. Several reasons have been presented in the literature to explain the tendency for the primary arm spacings to decrease with the decreasing growth speed near R_{max}. It has been attributed to the thermosolutal convection in the melt (refs. 6, 10 and 21). It has been suggested that this may be an artifact introduced in the primary arm size measurement technique, because of a change in the spatial distribution of primary dendrites, when the microstructure becomes cellular (ref. 10). It has been suggested that this maximum occurs at the cell to dendrite transition (ref. 16), in agreement with the experimental observation on succinonitrile-acetone alloy. However, data on aluminum-copper alloys (refs. 13 and 14) show that the cell to dendrite transition occurs in region B, at a growth speed between R_{min} and R_{max}. It has also been suggested that the contradictory behaviors reported in the literature may be because of the differing nature of the planar to cellular/dendritic transformation, i.e., whether the bifurcation is subcritical or supercritical (ref. 17).

In spite of the fact that growth speed and thermal gradient dependence of the primary arm spacings have been extensively reported, studies on the growth speed dependence of the primary arm spacings for the total range of the gradient of constitutional supercooling values, from almost zero (cellular microstructures found near the break down of a planar liquid-solid interface) to near unity (fully dendritic microstructures), are very limited (refs. 12 to 14 and 17). At a constant thermal gradient the exact growth speeds which correspond to the maxima in primary arm spacings are available only for Al-Cu (refs. 13 and 14) and succinonitrile-acetone (ref. 12). The partition coefficients for both these alloys are nearly the same, 0.14 for Al-2 wt % Cu (or 0.17 for Al-4 wt % Cu) and 0.1 for succinonitrile-5.5 mol % acetone. The magnitude of the partition coefficient is an important parameter in determining the extent of constitutional supercooling in the interdendritic melt near the tips of the primary array. Burden and Hunt (ref. 22) treated the composition gradient in the melt at the tip of primary dendrites (G_c^t) as made up of two components, the radial term ($\hat{G}_c$), related to curvature at the tip, and the planar term $\bar{G}_c$, due to the solute diffusing in the interdendritic melt towards the tip from behind. The ratio of these two contributions, $(\hat{G}_c/\bar{G}_c)$, is approximately equal to $k(1 - S^*)$ (refs. 2 and 22) for growth conditions, where the

solute Peclet number (Rr_t/D_l) is small (r_t is the radius of the primary dendrite at the tip). The increasing value of this ratio, ($\hat{G}_c/\bar{G}_c$), with increasing growth speed or ($1 - S^*$) may be responsible for the transition from planar to cellular and to dendritic morphologies. As this ratio is proportional to the solute partition coefficient an examination of the primary arm spacing maxima in several binary alloys with a range of partition coefficients is important for understanding the development of cellular/dendritic morphology and the associated primary arm spacing variations.

The purpose of this research was to examine the growth speed dependence of the primary arm spacings in a binary alloy with a relatively high partition coefficient, k. The alloy Pb-10 wt % Sn was selected because its k value (0.56) is very different from that in the other two alloys which have been investigated in detail, Al-2 wt % Cu (k = 0.14) (or Al-4 wt % Cu, k = 0.17) and succinonitrile-5.5 mol % acetone (k = 0.1). The whole range of the gradient of constitutional supercooling, ($1 - S^*$), from zero to unity was examined. This covers the growth conditions from R_p to beyond R_{max}, in order to investigate both, the cellular and the dendritic arrays.

EXPERIMENTAL

A charge of about 150 g, consisting of lead (99.99 % purity) and tin (99.99 % purity), was induction melted in an argon atmosphere in a quartz crucible. Direct coupling with the melt provided adequate mixing of the melt. The melt was superheated by about 40 K and pushed into four to six evacuated quartz tubes (0.6 cm i.d. and 0.8 cm o.d.) simultaneously, with the help of positive argon pressure, to obtain Pb-10 wt % Sn specimens for further directional solidification. The quartz tubes contained two chromel-alumel thermocouples (0.01 cm diam wires). These were located along the sample length with a separation distance of ~2 cm. They were kept in quartz sheaths (0.06 cm o.d.), closed at one end to protect them from the melt. The cast Pb-Sn specimens thus obtained were ~30 cm long. The quartz tubes containing these cast samples were then sealed at one end. These crucibles were evacuated and the cast specimens were remelted and directionally solidified. Directional solidification was carried out by raising the furnace assembly at various speeds (0.4 to 20 $\mu m\ s^{-1}$) with respect to the stationary sample, thus avoiding any convection caused by the crucible motion. Growth conditions were thermally stable, i.e., positive thermal gradient in the melt, with melt on top and the solid below. The furnace assembly, with an internal diameter of 1.3 cm, consisted of hot zone (20.3 cm long), insulating zone (1.3 cm long) and cold zone (7.0 cm long). The hot zone consisted of a sodium heat pipe kept within a resistance heated furnace. This helped maintain a ± 1 K control on the zone temperature. The middle insulated zone was made of alumina felt. The cold zone was a copper cylinder with internal channels through which flowed constant temperature (293 K) water at controlled flow rates (30 ml sec^{-1}). Temperatures within the sample were recorded by the help of the two thermocouples. The specimens were quenched after 12 to 14 cm of directional growth. The top thermocouple was approximately at the liquidus temperature (570 K) at quenching. For quenching, a jet of helium gas, cooled by liquid nitrogen, was directed to the surface of the quartz crucibles.

Specimens were metallographically polished and examined in the unetched condition. Longitudinal (parallel to growth direction) and transverse (perpendicular to growth direction) microstructures were examined by standard optical

metallography techniques. Primary arm spacings and their distribution were examined on the transverse sections. These sections were made in the quenched mushy region of the cellular/dendritic array, usually near the tips of the array. For some cellular specimens, these measurements were made on several sections along the quenched cell length. Two procedures were used in measuring the primary arm spacings. One method consisted of hand-counting the number (N) of cells/dendrites in an area and calculating $\lambda_1 = \sqrt{\text{Area}/N}$. About 160 to 350 cells/dendrites were counted for each measurement. In the other method, the cells or dendrites were traced by hand and the Cambridge Quantimet 900 Image Analyzer was used to obtain the detailed distribution of the perimeters of cell/dendrites. The average perimeter value was used to calculate the average size of the primary arms (λ_d), assumed to be equal to the diameter of a circle having equal perimeter. The tracings were also used to obtain a distribution of co-ordination number (number of nearest neighbor cells/dendrites) for primary arms.

RESULTS

Thermal Profiles

Figure 2 shows typical thermal profiles within the solidifying samples as recorded by the two thermocouples during directional solidification. The bottom and top thermocouples are denoted by TC number 1 and 2 respectively. Under thermal steady-state growth conditions, the two thermocouples will be expected to traverse identical thermal profiles. The two thermal profiles shown in figure 2(a) for a growth rate of 2 $\mu m\ sec^{-1}$ are identical except for their relative displacement on the abscissa. Thermal gradients in the melt at the dendrite tips, G_1, were obtained from such thermal profiles. Variation in the thermal gradient along the specimen length, corresponding to the profiles of figure 2(a), is shown in figure 2(b). The location of the eutectic and cell tip temperatures are represented with an accompanying sketch. As shown in this figure the temperature gradient is not constant in the mushy zone, as is usually assumed in analytical dendrite growth models. The gradient plots due to both thermocouples reproduce each other, showing that thermal steady-state was achieved in these experiments. In order to determine the effect of growth speed on the thermal gradient, plots of thermal gradient versus temperature for four different growth speeds are shown in figure 3. It is evident that the thermal profile within the sample is independent of the growth speed. It is determined by the imposed thermal profile of the furnace assembly, i.e., the hot zone and cold zone temperatures and the length of the insulated zone.

Microstructure

Typical microstructures of directionally solidified specimens are shown in figure 4. In figure 4(a) are shown longitudinal microstructures (parallel to the growth direction) for growth rates of 1.25 $\mu m\ sec^{-1}$ (fig. 4(a1)), 3.5 $\mu m\ sec^{-1}$ (fig. 4(a2)) and 4 $\mu m\ sec^{-1}$ (fig. 4(a3)). These correspond to a cellular microstructure near the planar-to-cellular transition, a cellular microstructure near the cell-to-dendrite transition and a dendritic microstructure, respectively. Examination of the quenched region of the cellular/dendritic array shows no evidence of uneven cell/dendrite lengths, referred to as "steepling" (refs. 5 and 23) in the literature. The cellular microstructure at the very lowest growth speed 1.25 $\mu m\ sec^{-1}$ (planar liquid-solid

interface was observed at a growth speed of 1 μm sec^{-1}) is atypical. The primary arm spacing distribution very close to the cell tips is not uniform. All other specimens had a more uniform cell/dendrite distribution at the tips. For all the cellular microstructures, i.e., at growth speeds below 4 μm sec^{-1}, the cell boundaries disappear as one moves from the cell tips towards their base, as has been reported for Al-2 wt % Cu (ref. 19). This would yield larger primary arm spacings, when measurements are made on transverse sections located well into the quenched mushy region. Hence for such microstructures, the primary arm spacings have been measured within 100 μm of the quenched tip. The dendritic microstructures obtained at growth speeds of 4 μm sec^{-1} and higher, did not show such a behavior (figs. 4(a2) and (a3)).

The corresponding transverse microstructures (perpendicular to the growth direction) are shown in figure 4(b). The microstructure at 1.25 μm sec^{-1} contains two type of regions, one consisting of a continuous net-work of uniformly distributed primary cells and the other of cell-boundaries that are not well defined. This behavior is not observed at higher growth speeds, where uniformly distributed cells (fig. 4(b2)) and dendrites (fig. 4(b3)) are observed throughout the transverse section. Tin precipitates were observed both, within the cells/dendrites (because of the solid-state precipitation) and in the intercellular/interdendritic region. The intercellular boundaries are delineated by fine tin particles (fig. 4(b2)), whereas, the dendritic microstructures show larger tin particles located at the dendrite-nodes, and much finer particles around the dendrite peripheries (fig. 4(b3)).

PRIMARY CELL/DENDRITE ARMS

Primary Arm Size Distribution

A typical variation in the distribution of primary arm sizes as a function of growth speed is shown in figure 5 (plotted as perimeter distribution as obtained from the Quantimet). At very low growth speeds near the planar to cellular transition (2 μm sec^{-1}, fig. 5(a)), the perimeter distribution is widest. The distribution becomes narrower as the growth speed increases for the cellular morphology (compare figs. 5(a) and (b)). At growth conditions just beyond the cell to dendrite (branched cell) transition, the perimeter distribution becomes more Gaussian (compare Figs. 5(b) and 5(c)). The Gaussian distribution of the perimeter is more or less maintained for the dendritic microstructures grown at higher speeds, however the distribution width appears to increase (fig. 5(d)). As mentioned before, the average perimeter values from plots as shown in figure 5, have been used to obtain the average primary cell/dendrite sizes (λ_d).

Results of the perimeter distribution measurements along the length of a dendritic sample directionally solidified at 10 μm sec^{-1} show no significant variation in primary arm size and its distribution (fig. 6). Two typical perimeter distributions corresponding to the cross-sections, located at 1.8 and 4.8 cm from the quenched tip, are shown in figure 6. The average λ_d values for these sections is 130 and 142 μm respectively. Observation of constant primary arm spacings along the length of the directionally solidified specimen also establishes that steady-state growth conditions were achieved during directional solidification of these specimens.

Co-ordination Number

Figure 7 shows typical co-ordination number distributions obtained for the cellular and dendritic microstructures. The filled symbols are for the dendritic microstructures. The open symbols are for cells. Nearly perfect hexagonal arrangements (co-ordination number = 6) are obtained for cellular microstructures only near the cell to dendrite transition ($R = 3.5\ \mu m\ sec^{-1}$). Cells grown at lower growth speeds have co-ordination number between five and six ($R = 1.5, 2, 3\ \mu m\ sec^{-1}$). The dendritic microstructures have the most frequent co-ordination numbers between four and five ($R = 4, 5, 20\ \mu m\ sec^{-1}$). A summary of the growth speed dependence of the most frequently observed co-ordination numbers and their standard deviation (as given by the half-peak heights in fig. 7) is presented in figure 7(b). Differences in the spatial distribution of cells formed at various growth speeds are not significant. However, it appears (considering the scatter in the data) that the average co-ordination number of dendrites is smaller, about 4.5 as compared to about 5.5 for cells.

Primary Arm Spacings

Growth speed dependence of the primary arm spacings in Pb-10 wt % Sn is shown in figure 8. The growth regime examined in this study, spans speeds very close to the break-down of the planar liquid-solid interface, $1.25\ \mu m\ sec^{-1}$ (R_p was experimentally observed to be $1\ \mu m\ sec^{-1}$), to the fully dendritic morphology at higher growth rates, $20\ \mu m\ sec^{-1}$. The circles represent the primary arm spacing (λ_1) and the squares represent the primary arm size (λ_d) as obtained from Quantimet measurements. The scatter in λ_d values are also indicated. The filled symbols correspond to the dendritic microstructures and the open symbols are for the cellular microstructure. The solid line is drawn to depict the average growth rate dependence of the primary arm spacing. The growth speed for the planar liquid-solid interface is indicated by R_p. Starting from higher growth rates, the primary arm spacing increases at first, with decreasing growth rate, reaches a maximum and then decreases with further decrease in growth rate. However, it does not show the behavior reported in Al-4 wt % Cu (ref. 13) and succinonitrile-acetone (ref. 17), where a minimum in primary arm spacings was observed (at R_{min} shown schematically in fig. 1).

Figure 9 shows that the average primary arm sizes (λ_d), as given by the diameter of a circle with equivalent perimeter as the cells/dendrites, are about the same as the arm spacings, λ_1, which were obtained by counting the primary arms in a given area ($\sqrt{Area/N}$). The ratio λ_d/λ_1 is approximately unity for both, the cellular and the dendritic microstructures. This observation suggests that the experimentally observed decrease in arm spacings with the decreasing growth speeds near R_{max}, is real. It is not an artifact, attributed to the spatial distribution differences between dendrites and cells, as has been suggested in the literature (ref. 10).

As seen before (figs. 7(a) and (b)), the spatial distribution of cellular microstructures is independent of growth speed. Hence the decrease in primary arm spacings for the cellular microstructures can not be attributed to differences in spatial distribution of primary arms. The small difference between the spatial distribution of cells and dendrites (co-ordination number of cells = 5.5 and dendrites = 4.5, fig. 7(b)) can not account for the different growth rate dependence of the dendritic and cellular microstructures.

Cell to Dendrite Transition

We will define the cell to dendrite transition, as the smallest growth speed at which the dendritic microstructure is observed, for an alloy grown at a constant thermal gradient. The dendrites, as identified with the formation of first side branches on the sides of the cellular array, were observed to occur at 4 $\mu m\ sec^{-1}$ and higher speeds. Only cellular microstructures were observed at smaller growth speeds. The maximum in the primary arm spacing also occurs at 4 $\mu m\ sec^{-1}$. The cell to dendrite transition coincides with the primary arm spacing maximum, as has been reported in succinonitrile-acetone (ref. 16). However, this behavior, seen here in Pb-Sn, is different from that reported in Al-4 wt % Cu (ref. 13) and Al-2 wt % Cu (ref. 14), where the cell to dendrite transition was observed to occur at growth speeds smaller than the one corresponding to the primary arm spacing maximum.

DISCUSSION

Influence of Solute Partition Coefficient

The role of partition coefficient in determining the growth speed at which the maximum in primary arm spacings is observed in binary alloys can be examined in terms of the gradient of constitutional supercooling ($1 - S^*$) values. Figure 10 plots the magnitude of the solute partition coefficients versus ($1 - S^*$), at which the maxima in primary arm spacings have been observed. The data available in the literature, succinonitrile-5.5 mol % acetone (refs. 12 and 16), Al-4 wt % Cu (refs. 13 and 14) and Al-2 wt % Cu (ref. 14) are compared with the behavior observed in this study for Pb-10 wt % Sn. The primary arm spacing maxima occur at gradient of constitutional supercooling, ($1 - S^*$), values of about 0.89 to 0.99 for alloys with small partition coefficients, $k = 0.1$ to 0.17. Whereas for Pb-Sn with a higher partition coefficient (0.56) the primary arm spacing maximum occurs at a much smaller value of ($1 - S^*$), 0.63.

It also appears that the magnitude of partition coefficient has a definite influence on the nature of the planar to cellular bifurcation. Absence of region "A" (shown schematically in fig. 1) in the growth speed dependence of the primary arm spacings (fig. 8), suggests that for the Pb-10 wt % Sn alloy the planar to cellular bifurcation is supercritical. This is different from Al-4.1 wt % Cu (ref. 13) and succinonitrile-acetone (ref. 17) alloys, where a well defined "A" type of region has been observed. By examining the nonlinear stability analysis for break-down of a planar liquid-solid interface, Wollkind and Segel (ref. 24), Coroli et al. (ref. 25) have suggested that the magnitude of partition coefficient is critical, in determining whether the planar to cellular bifurcation is supercritical or subcritical. By assuming the liquid and solid thermal conductivities to be equal, the subcritical bifurcations are predicted for alloys with the solute partition coefficients less than 0.45 (refs. 25 and 26). This is in agreement with the behavior in Al-Cu ($k = 0.17$) and succinonitrile-acetone ($k = 0.1$). The present observation of supercritical bifurcation in Pb-Sn ($k = 0.56$) further strengthens the above mentioned theoretical approach (ref. 25). However, it is necessary to confirm this behavior by examining at least one more binary alloy with $k > 0.45$.

Comparison With Primary Arm Spacing Model

Two approaches have been taken in the literature to model the growth speed and thermal gradient dependence of primary arm spacings. In the first approach the Bower, Brody and Flemings (ref. 27) microsegregation model for a primary dendrite array was extended by Hunt (ref. 3) to obtain the following relationship,

$$\lambda_1^2 = 4\sqrt{2}\,[(G_c^t/\bar{G}_c) - 1]\,(D_l/R)\,r_t \quad . \quad . \quad . \qquad (1)$$

The solutal gradient in the melt at the dendrite tip, G_c^t, and r_t relationships from dendrite growth models (refs. 2, 22 and 28) have been used by investigators with the above relationship to predict the growth speed and thermal gradient dependence of primary arm spacings. The dendrite growth model of Trivedi (ref. 28) assumes a paraboloidal dendrite tip, and is valid only for the dendritic morphologies. The models by Burden and Hunt (ref. 22) and Laxmanan (ref. 2) do not distinguish between cell and dendrite. These are based on an assumption that the curvature contribution to the solutal gradient at the tip decays over a distance proportional to the tip radius. The other recent approach in the literature (ref. 29) is valid for a two dimensional cellular array and relates the ratio, λ_1/r_t, to the gradient of constitutional supercooling. In the following, instead of going into a detailed comparison with predictions from several models, let us examine only the cellular array model of Hunt (ref. 3). We will use the effective thermal gradient, G, instead of the gradient in the liquid, G_l, as used by Hunt. The experimental observations are compared with the theoretical predictions in figure 11, where the primary arm spacings are plotted as a function of $(1 - S^*)$, the gradient of constitutional supercooling. The quantitative agreement is good at higher gradients of constitutional supercoolings for dendritic microstructures. However, the model overpredicts the primary arm spacings for the cellular microstructures at low gradients of constitutional supercoolings. The "A" type of region at small $(1 - S^*)$ values, shown schematically in figure 1 near the planar to cellular break-down regime, is not predicted by this model. This trend agrees with the present experimental observations.

The influence of thermosolutal convection on the experimentally observed growth speed dependence of primary arm spacings, however, remains unexplored. The Pb-10 wt % Sn alloy specimens have been directionally solidified under growth conditions which are expected to be solutally unstable. The solutal convection in these samples can arise from two contributions. First is the convection in the interdendritic melt because of the increasing solute content (decreasing melt density) from the tips of primary array to its base at the eutectic temperature. The second is the convection in the melt ahead of the tips caused by the solutal build-up at the tips. Both these effects are expected to cause macrosegregation in the transverse and the longitudinal directions. It is expected that the interdendritic convection will not be present in Pb-10 wt % Sn samples, because of the geometrical constraints imposed by the very small volume fraction of interdendritic melt. However, the convection from the solutal build up at the tips, especially for the cellular arrays growing at very low gradients of constitutional supercoolings, is likely to affect the array morphology. This may be the reason for the poor quantitative agreement between the theoretically predicted and the experimentally observed arm spacings for the cellular microstructures (fig. 11). Macrosegregation studies are in progress to investigate this effect.

SUMMARY

Primary arm spacings have been examined in this study for the cellular/dendritic arrays growing during directional solidification of Pb-10 wt % Sn. For a constant thermal gradient, G_l = 110 K cm^{-1} at the cell/dendrite tips, the growth speed has been varied to study the whole range of the gradient of constitutional supercooling values, from close to zero (cellular microstructures near the break-down of the planar liquid-solid interface) to near/unity (fully dendritic microstructures at higher growth speeds). Careful experimental control and thermal measurements have been used to ensure a thermal steady-state growth of primary arm spacings. Primary arm spacings (λ_1), primary arm size (λ_d) and their distribution have been examined by detailed quantitative measurements. The following conclusions can be drawn from this study.

1. Decrease in growth speed (R) results in increasing primary arm spacings for the dendritic microstructures, until a maximum is observed in primary arm spacings at R_{max}. This maximum is real and is not an artifact introduced from differences in the spatial arrangement of primary arms for the cells and dendrites.

2. Spatial arrangements of cells and dendrites, as observed from their co-ordination number distribution on transverse sections, are not very different.

3. The magnitude of the solute partition coefficient (k) has a large influence on the development of the cellular or dendritic array.

(a) The primary arm spacing maximum in Pb-Sn alloy with a large k value (k = 0.56) occurs at a much lower gradient of constitutional supercooling [(1 - S*)] = 0.68), as compared to Al-Cu (k = 0.14 for 2 wt % and 0.17 for 4 wt % Cu) and succinonitrile-acetone (k = 0.1) [(1 - S*) = 0.89 to 0.99)].

(b) The planar to cellular bifurcation in Pb-Sn is supercritical as compared to the subcritical bifurcations in Al-Cu and succinonitrile-acetone. This behavior is expected from the instability models which use nonlinear analysis to describe the break-down of a planar liquid-solid interface (refs. 24 and 25).

4. The experimentally observed variation in primary arm spacings has the trend predicted by the model due to Hunt (3) for the total growth regime, cells near initial break-down of the planar interface to dendrites at high growth speeds. The quantitative agreement with the data is good for the dendritic microstructures at higher gradients of supercoolings. However, for the cellular microstructures the model overpredicts the arm spacings.

ACKNOWLEDGEMENT

This research was carried-out at the Microgravity Materials Science Laboratory of NASA-Lewis Research Center, Cleveland, Ohio with support from the Microgravity Science and Applications Division (CODE EN), NASA Headquarters, Washington, DC (Grant NCC-395). Appreciation is expressed to Steve White, M. Vijayakumar, Jerry Loveland and Richard Rauser for their assistance and to

Thomas K. Glasgow, Chief, Processing Science and Technology Branch, for his continued support and encouragement.

REFERENCES

1. Mullins, W.W., and Sekerka, R.F., "Stability of a Planar Interface During Solidification of a Dilute Binary Alloy," Journal of Applied Physics, Vol. 35, 1964, pp. 444-451.

2. Laxmanan, V., "Cellular and Dendritic Growth in a Binary Alloy Melt: A Marginal Stability Approach," Journal of Crystal Growth, Vol. 75, 1986, pp. 573-580.

3. Hunt, J.D., Solidification and Casting of Metals, The Metals Society, London, 1979, p. 3.

4. Mason, J.T., Verhoeven J.D., and Trivedi, R., "Primary Dendrite Spacing: Part II. Experimental Studies of Pb-Pd and Pb-Au Alloys," Metallurgical Transactions A, Vol. 15A, No. 9, Sept. 1984, pp. 1665-1676.

5. Verhoeven, J.D., Mason, J.T., and Trivedi, R., "The Effect of Convection on the Dendrite to Eutectic Transition," Metallurgical Transactions A, Vol. 17A, No. 6, June 1986, pp. 991-1000.

6. Mason, J.T., Verhoeven, J.D., and Trivedi, R., "Primary Dendrite Spacing. I. Experimental Studies," Journal of Crystal Growth, Vol. 59, 1982, pp. 516-524.

7. Jin, I., and Purdy, G.R., "Controlled Solidification of a Dilute Binary Alloy," Journal of Crystal Growth, Vol. 23, 1974, pp. 29-44.

8. Okamoto, T., and Kishitaka, K., "Dendritic Structure in Unidirectionally Solidified Aluminum, Tin, and Zinc Base Binary Alloys", Journal of Crystal Growth, Vol. 29, 1975, pp. 137-146.

9. Young, K.P., and Kirkwood, D.H., "The Dendrite Arm Spacings of Aluminum-Copper Alloys Solidified Under Steady-State Conditions," Metallurgical Transactions A, Vol. 6A, No. 1, Jan. 1975, pp. 197-205.

10. McCartney, D.G., and Hunt, J.D., "Measurements of Cell and Primary Dendrite Arm Spacings in Directionally Solidified Aluminum Alloys," Acta Metallurgica, Vol. 29, No. 11, Nov. 1981, pp. 1851-1863.

11. Klaren, C.M., Verhoeven, J.D., and Trivedi, R., "Primary Dendrite Spacing of Lead Dendrites in Pb-Sn and Pb-Au Alloys," Metallurgical Transactions A, Vol. 11A, No. 11, Nov. 1980, pp. 1853-1861.

12. Somboonsuk, K., Mason, J.T., and Trivedi, R., "Interdendrite Spacing: Part I. Experimental Studies," Metallurgical Transactions A, Vol. 15A, No. 6, June 1984, pp. 967-975.

13. Miyata, Y., Suzuki, T., and Uno, J.I., "Cellular and Dendritic Growth: Part I. Experiment," Metallurgical Transactions A, Vol. 16A, No. 10, Oct. 1985, pp. 1799-1805.

14. An Geying and Liu Lixin, "Dendrite Spacing in Unidirectionally Solidified Al-Cu Alloy," Journal of Crystal Growth, Vol. 80, 1987, pp. 383-392.

15. Esaka, H., and Kurz, W., "Columnar Dendrite Growth: Experiments on Tip Growth," Journal of Crystal Growth, Vol. 72, 1985, pp. 578-584.

16. Trivedi, R., "Interdendrite Spacing: Part II. A Comparison of Theory and Experiment," Metallurgical Transactions A, Vol. 15A, No. 6, June 1984, pp. 977-982.

17. Eshelman, M.A., Seetharaman, V., and Trivedi, R., "Cellular Spacings - I. Steady-State Growth," Acta Metallurgica, Vol. 36, No. 4, Apr. 1988, pp. 1165-1174.

18. Jamgotchian, H., Billia, B., and Capella, L., "Morphology of the Solidification Front During Unidirectional Growth of Pb-Tl Alloys," Journal of Crystal Growth, Vol. 64, 1983, pp. 338-344.

19A. Sharp, R.M., and Hellawell, A., "Solute Distributions at Non-Planar, Solid-Liquid Growth Fronts. I. Steady-State Conditions," Journal of Crystal Growth, Vol. 6, 1970, pp. 253-260.

19B. Sharp, R.M., and Hellawell, A., "Solute Distributions at Non-Planar, Solid-Liquid Growth Fronts. I. Steady-State Conditions," Journal of Crystal Growth, vol. 11, 1971, pp. 77-91.

20. Tewari, S.N., and Laxmanan, V., "A Critical Examination of the Dendrite Growth Models: Comparison of Theory With Experimental Data," Acta Metallurgica, Vol. 35, No. 1, Jan. 1987, pp. 175-183.

21. Dupouy, M.D., Camel,D., and Favier, J.J., "Natural Convection in Directional Dendritic Solidification of Metallic Alloys - I. Macroscopic Effects," Acta Metallurgica, Vol. 37, No. 4, Apr. 1989, pp. 1143-1157.

22. Burden, M.H., and Hunt, J.D., "Cellular and Dendritic Growth," Journal of Crystal Growth, Vol. 22, 1974, pp. 99-116.

23. Burden, M.H., Hebditch, D.J., and Hunt, J.D., "Macroscopic Stability of a Planar, Cellular or Dendritic Interface During Directional Freezing," Journal of Crystal Growth, Vol. 20, 1973, pp. 121-124.

24. Wollkind, D., and Segel, L., "A Nonlinear Stability Analysis of the freezing of a Dilute Binary Alloy," Philosophical Transactions of the Royal Society of London, Vol. 268, No. 1191, Dec 24, 1970, pp. 351-380.

25. Caroli, B., Coroli, C., and Roulet, B., "On the Emergency of One-Dimensional Front Instabilities in Directional Solidification and Fusion of Binary Mixtures," Journal de Physique, Vol. 43, No. 12, 1982, pp. 1767-1780.

26. Eshelman, M.A., and Trivedi, R., "The Planar to Cellular Transition During the Directional Solidification of Alloys," Acta Metallurgica, Vol. 35, No. 10, Oct. 1987, pp. 2443-2452.

27. Bower, T.F., Brody, H.D., and Flemings, M.C., "Measurements of Solute Redistribution in Dendritic Solidification," Transactions of the American Institute of Mining Engineers, Vol. 236, No. 5, May 1966, pp. 624-634.

28. Trivedi, R., "Theory of Dendritic Growth During the Directional Solidification," Journal of Crystal Growth, Vol. 49, 1980, pp. 219-232.

29. Billia, B., Jamgotchian, H., and Capella, L., "Pattern Selection During Directional Solidification," Journal of Crystal Growth, Vol. 82, 1987, pp. 747-756.

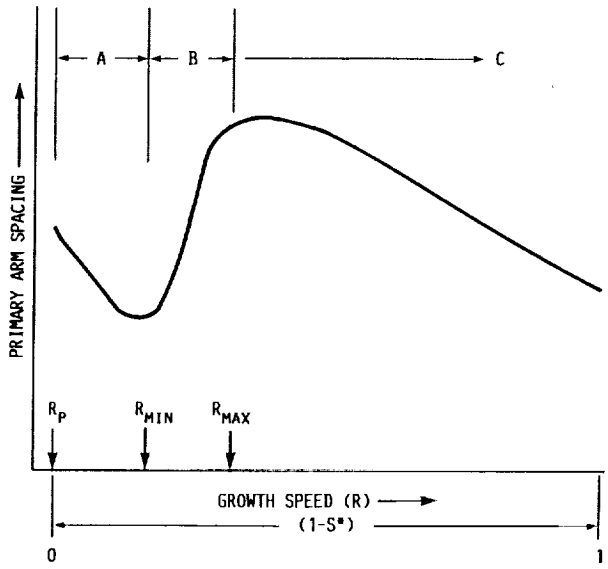

FIGURE 1. - SCHEMATIC REPRESENTATION OF GROWTH SPEED DEPENDENCE OF PRIMARY ARM SPACINGS DURING CONSTRAINED GROWTH OF BINARY ALLOYS. (1-S*) DENOTES THE GRADIENT OF CONSTITUTIONAL SUPERCOOLING.

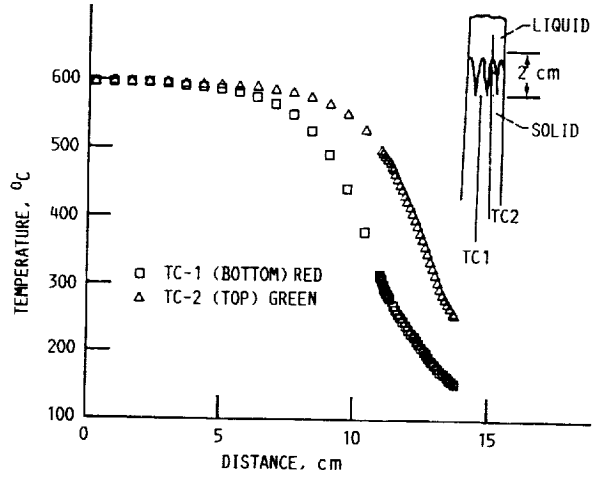

(a) TEMPERATURES AS RECORDED BY TWO THERMOCOUPLES, LOCATED WITHIN THE SAMPLE WITH AN AXIAL SPACING OF ABOUT 2 CM.

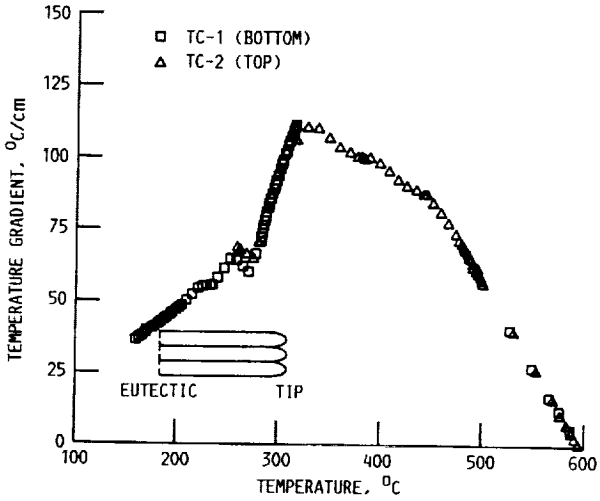

(b) STEADY STATE THERMAL PROFILE WITHIN THE SAMPLE DURING DIRECTIONAL SOLIDIFICATION THERMAL GRADIENT VERSUS TEMPERATURE PLOT.

FIGURE 2. - TYPICAL THERMAL PROFILES, WITHIN THE SPECIMEN DURING DIRECTIONAL SOLIDIFICATION OF Pb-10 WT % Sn.

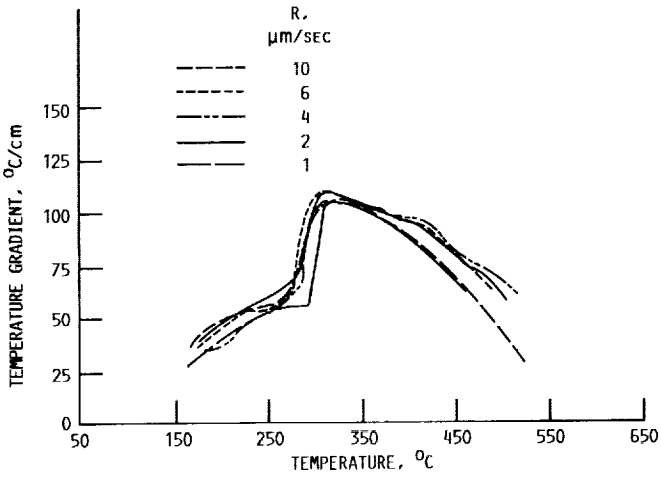

FIGURE 3. - THERMAL PROFILES WITHIN THE SAMPLE ARE INDEPENDENT OF GROWTH SPEED. THE IMPOSED THERMAL PROFILE OF THE FURNACE ASSEMBLY DETERMINES THE THERMAL PROFILE OF THE SAMPLE.

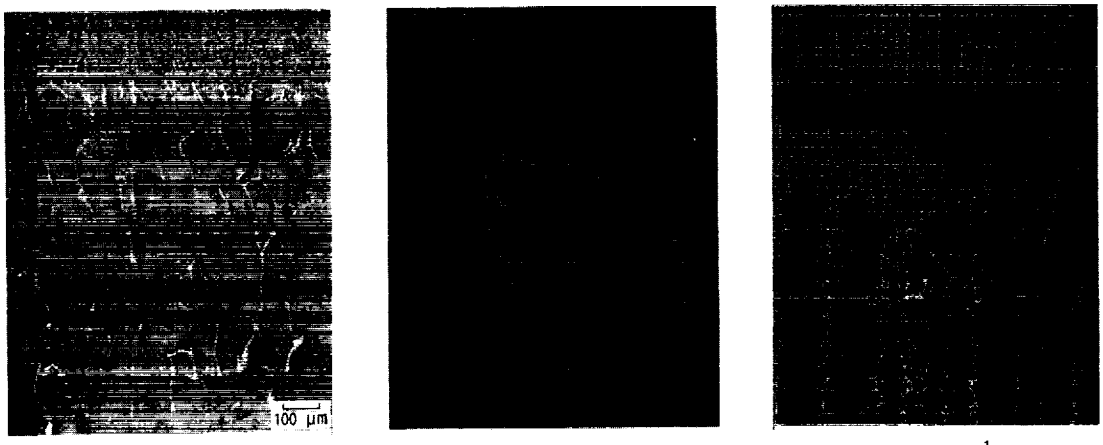

(i) 1.25 μm s^{-1}. (ii) 3.5 μm s^{-1}. (iii) 4 μm s^{-1}.

(a) LONGITUDINAL (PARALLEL TO THE GROWTH DIRECTION).

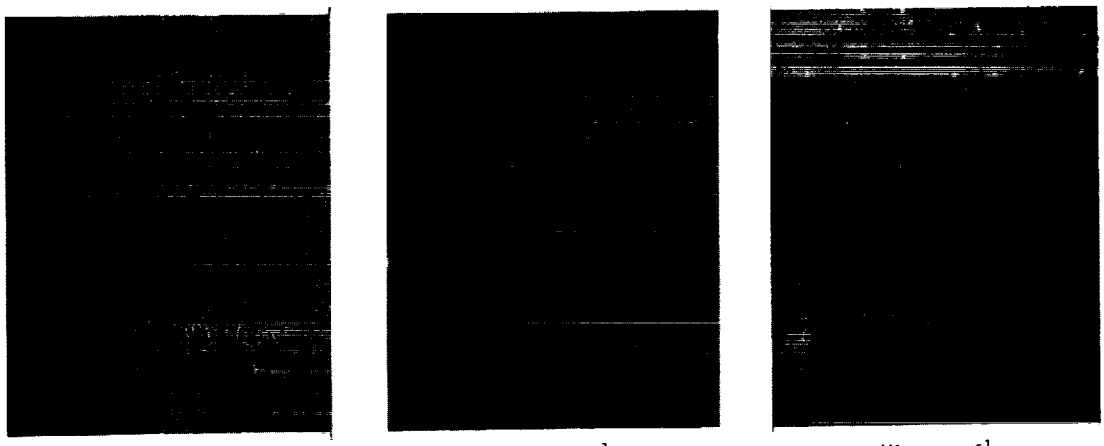

(i) 1.25 μm s^{-1}. (ii) 3.5 μm s^{-1}. (iii) 4 μm s^{-1}.

(b) TRANSVERSE (PERPENDICULAR TO THE GROWTH DIRECTION).

FIGURE 4. - TYPICAL MICROSTRUCTURES OF DIRECTIONALLY SOLIDIFIED SPECIMENS.

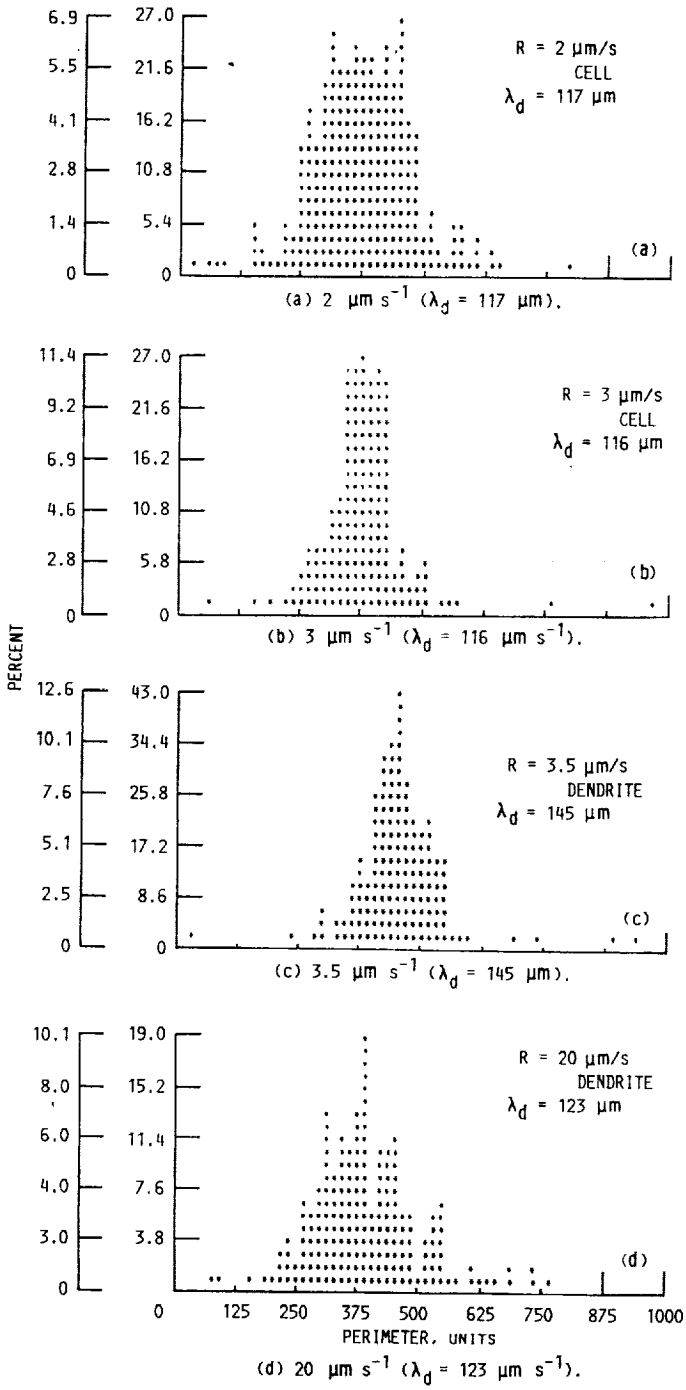

FIGURE 5. - GROWTH SPEED DEPENDENCE OF PRIMARY ARM SIZE (PERIMETER) DISTRIBUTION IN DIRECTIONALLY SOLIDIFIED Pb-10 wt PERCENT Sn . THE EQUIVALENT DIAMETER FOR A CIRCLE HAVING THE AVERAGE PERIMETER VALUE FROM SUCH PLOTS HAS BEEN USED AS THE AVERAGE ARM SIZES, λ_d.

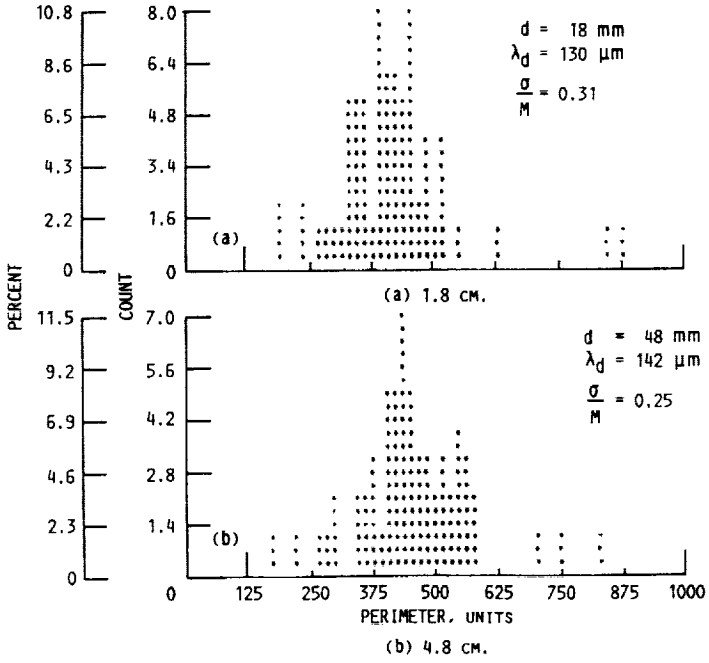

FIGURE 6. - PRIMARY ARM SIZE DISTRIBUTION (PERIMETER DISTRIBUTION) IS CONSTANT ALONG THE LENGTH OF THE DIRECTIONALLY SOLIDIFIED SAMPLE (GROWTH SPEED = 10 μm s^{-1}). THESE DISTRIBUTIONS REPRESENT CROSS SECTIONS LOCATED FROM THE QUENCHED DENDRITE TIPS.

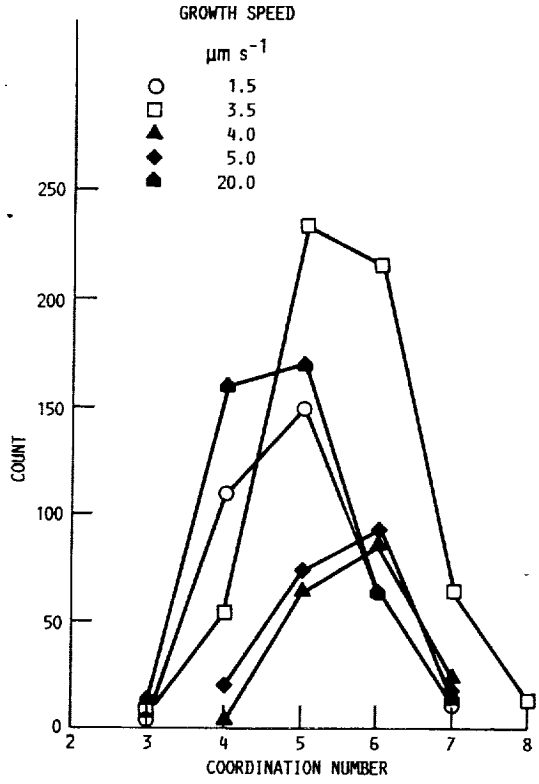

(a) DISTRIBUTION OF COORDINATION NUMBERS.

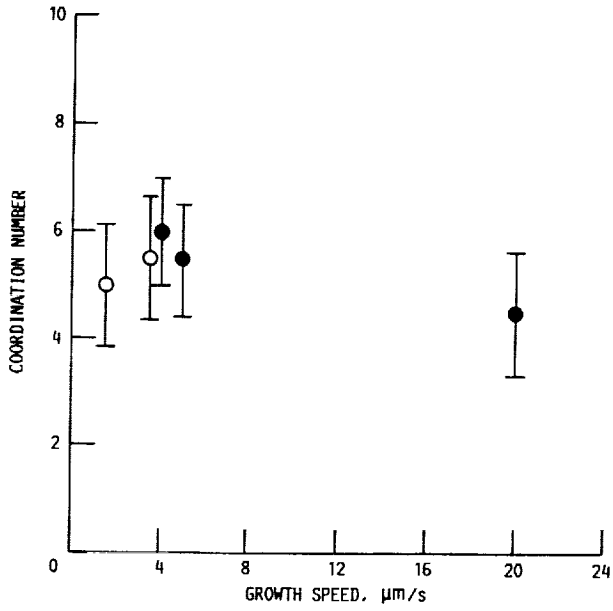

(b) VARIATION OF AVERAGE COORDINATION NUMBER WITH GROWTH SPEED.

FIGURE 7. - EFFECT OF GROWTH SPEED ON SPATIAL DISTRIBUTION OF PRIMARY CELLS/DENDRITES. FILLED SYMBOLS FOR DENDRITES AND OPEN SYMBOLS FOR CELLS.

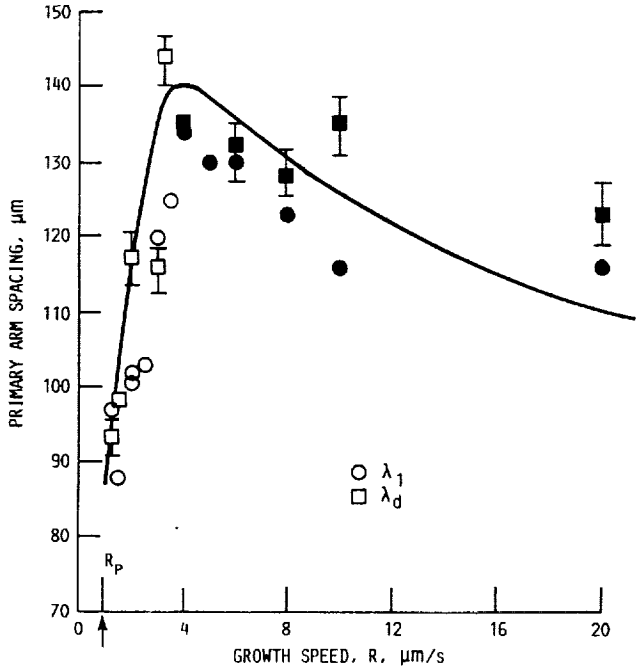

FIGURE 8. - GROWTH SPEED DEPENDENCE OF PRIMARY ARM SPACINGS (λ_1) (CIRCLES) AND PRIMARY ARM SIZE (λ_d) (SQUARES) IN DIRECTIONALLY SOLIDIFIED Pb-10 WT PERCENT Sn. FILLED SYMBOLS FOR DENDRITES AND OPEN SYMBOLS FOR CELLS.

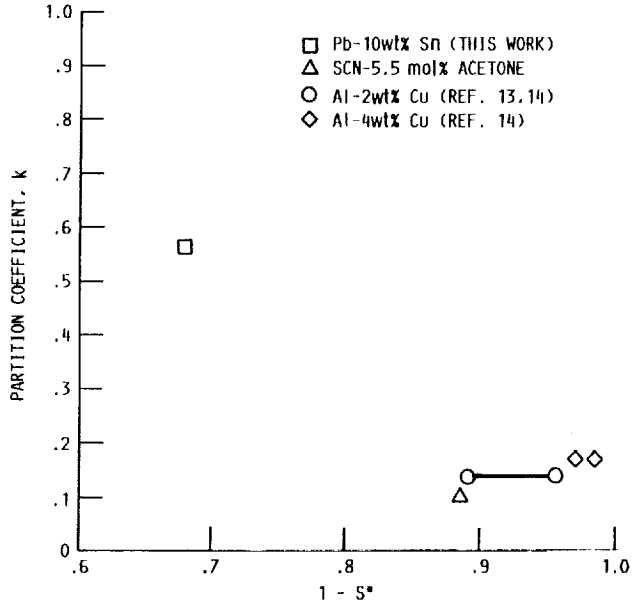

FIGURE 10. - PARTITION COEFFICIENT VERSUS THE GRADIENT OF CONSTITUTIONAL SUPERCOOLING AT WHICH THE MAXIMUM IN PRIMARY ARM SPACINGS OCCURS.

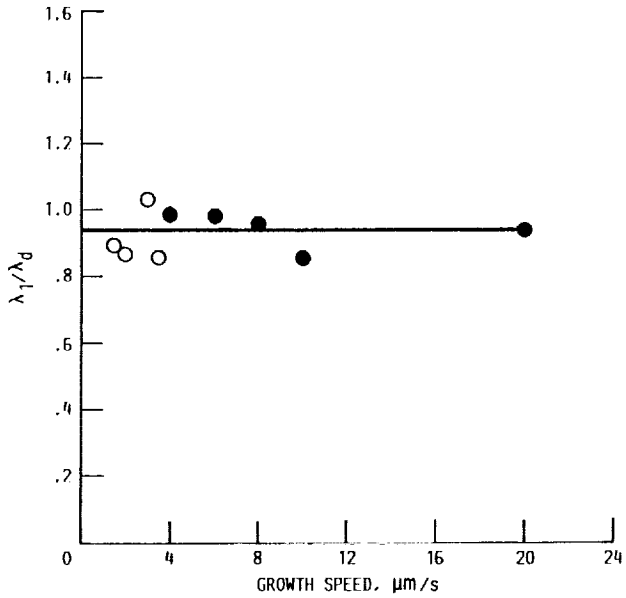

FIGURE 9. - EQUIVALENCE BETWEEN PRIMARY ARM SIZE (λ_d) AND PRIMARY ARM SPACINGS (λ_1) FOR THE CELLULAR AND DENDRITIC ARRAYS. FILLED SYMBOLS FOR DENDRITES AND OPEN SYMBOLS FOR CELLS.

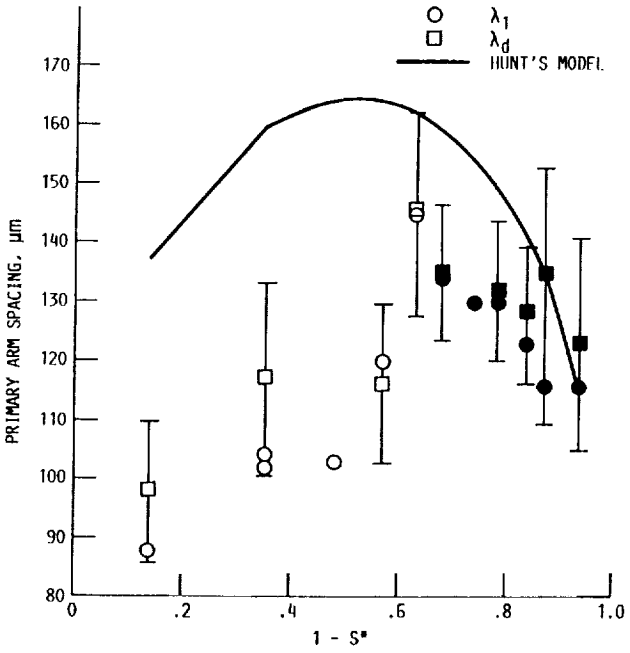

FIGURE 11. - COMPARISON OF THE EXPERIMENTALLY OBSERVED DEPENDENCE OF PRIMARY ARM SPACINGS ON (1-S*), THE GRADIENT OF CONSTITUTIONAL SUPERCOOLING, WITH THEORETICAL PREDICTION FROM THE MODEL BY HUNT (REF. 3).

NASA
National Aeronautics and Space Administration

Report Documentation Page

1. Report No.	2. Government Accession No.	3. Recipient's Catalog No.
NASA CR-185190 AIAA-90-0740		

4. Title and Subtitle

Primary Arm Spacing in Directionally Solidified Pb-10 wt % Sn Alloys

5. Report Date

January 1990

6. Performing Organization Code

7. Author(s)

M. A. Chopra and S. N. Tewari

8. Performing Organization Report No.

None (E-5141)

10. Work Unit No.

674-25-05

9. Performing Organization Name and Address

Cleveland State University
Chemical Engineering Department
Cleveland, Ohio 44115

11. Contract or Grant No.

NCC3-95

13. Type of Report and Period Covered

Contractor Report
Final

12. Sponsoring Agency Name and Address

National Aeronautics and Space Administration
Lewis Research Center
Cleveland, Ohio 44135-3191

14. Sponsoring Agency Code

15. Supplementary Notes

Project Manager, Thomas K. Glasgow, Materials Division, NASA Lewis Research Center. Prepared for the 28th Aerospace Sciences Meeting sponsored by the American Institute of Aeronautics and Astronautics, Reno, Nevada, January 8-11, 1990. M. A. Chopra, Cleveland State University and NASA Resident Research Scientist at Lewis Research Center; S. N. Tewari, Associate Professor, Cleveland State University.

16. Abstract

The dependence of primary arm spacings on growth speed has been investigated for cellular and dendritic arrays in Pb-10 wt % Sn samples directionally solidified under a constant positive thermal gradient in the melt. The gradient of constitutional supercooling has been varied from almost zero (near the break-down of the planar liquid-solid interface at small growth speeds, cellular morphology) to near unity (large growth speeds, dendritic morphology). The spatial arrangements of cells and dendrites, as given by their co-ordination number, are not very different from each other. It appears that primary arm spacing maxima and the cell to dendrite transition are strongly influenced by the magnitude of the solute partition coefficient. The planar to cellular bifurcation is supercritical in Pb-Sn which has a high partition coefficient, as compared to the subcritical behavior reported in Al-Cu and succinonitrile-acetone, both of which have low partition coefficients. The primary arm spacing model due to Hunt agrees with the experimentally observed trend for the whole growth regime. There is a good quantitative agreement at higher gradients of supercooling. However, the model overpredicts the primary arm spacings at low gradients of constitutional supercooling.

17. Key Words (Suggested by Author(s))	18. Distribution Statement
Solidification Dendritic growth Constitutional supercooling	Unclassified - Unlimited Subject Category 29

19. Security Classif. (of this report)	20. Security Classif. (of this page)	21. No. of pages	22. Price*
Unclassified	Unclassified	18	A03

*For sale by the National Technical Information Service, Springfield, Virginia 22161